Evaluation of standard imaging techniques and volumetric preservation of nervous tissue in genetically identical offspring of the crayfish *Procambarus fallax* cf. *virginalis* (Marmorkrebs)

Emanuel S Nischik [1] , Jakob Krieger [Corresp. 1]

1 Zoological Institute and Museum, Cytology and Evolutionary Biology, University of Greifswald, Greifswald, Germany

Corresponding Author: Jakob Krieger
Email address: jakob.krieger@uni-greifswald.de

In the field of comparative neuroanatomy, a meaningful interspecific comparison demands quantitative data referring to method-specific artifacts. For evaluating the potential of state-of-the-art imaging techniques in arthropod neuroanatomy, micro-computed X-ray microscopy (µCT) and two different approaches using confocal laser-scanning microscopy (cLSM) were applied to obtain volumetric data of the brain and selected neuropils in *Procambarus fallax* forma *virginalis* (Crustacea, Malacostraca, Decapoda). The marbled crayfish *P. fallax* cf. *virginalis* features a parthogenetic reproduction generating genetically identical offspring from unfertilized eggs. Therefore, the studied organism provides ideal conditions for the comparative analysis of neuroanatomical imaging techniques and the effect of preceding sample preparations of nervous tissue. We found that wet scanning of whole animals, conducted with µCT turned out to be the least disruptive method. However, in an additional experiment it was discovered that fixation in Bouin's solution, required for µCT scans, resulted in an average tissue shrinkage of 24 % compared to freshly dissected and unfixed brains. The complete sample preparation using fixation in half-strength Karnovsky's solution of dissected brains led to an additional volume decrease of 12.5 %, whereas the preparation using zinc-formaldehyde as fixative resulted in a shrinkage of 5 % in comparison to the volumes obtained by µCT. By minimizing individual variability, at least for aquatic arthropods, this pioneer study aims for the inference of method-based conversion factors in the future, providing a valuable tool for reducing quantitative neuroanatomical data already published to a common denominator. However, volumetric deviations could be shown for all experimental protocols due to methodological noise and/or phenotypic plasticity among genetically identical individuals. Micro-computed X-ray microscopy using undried tissue is an appropriate non-disruptive technique for allometry of arthropod brains since spatial organ relationships are conserved and tissue shrinkage is minimized. Collecting tissue-based shrinkage factors according to specific sample

preparations might allow a better comparability of volumetric data from the literature, even if another technique was applied.

1 **Evaluation of standard imaging techniques and volumetric preservation of**

2 **nervous tissue in genetically identical offspring of the crayfish *Procambarus***

3 ***fallax* cf. *virginalis* (Marmorkrebs)**

6 EMANUEL SET NISCHIK[1] AND JAKOB KRIEGER[1*]

7 [1] University of Greifswald, Zoological Institute and Museum, Cytology and Evolutionary

8 Biology, Soldmannstraße 23, 17489 Greifswald

9 Contact: en122971@uni-greifswald.de; jakob.krieger@uni-greifswald.de

11 [*]corresponding author

Abstract

In the field of comparative neuroanatomy, a meaningful interspecific comparison demands quantitative data referring to method-specific artifacts. For evaluating the potential of state-of-the-art imaging techniques in arthropod neuroanatomy, micro-computed X-ray microscopy (μCT) and two different approaches using confocal laser-scanning microscopy (cLSM) were applied to obtain volumetric data of the brain and selected neuropils in *Procambarus fallax* forma *virginalis* (Crustacea, Malacostraca, Decapoda). The marbled crayfish *P. fallax* cf. *virginalis* features a parthogenetic reproduction generating genetically identical offspring from unfertilized eggs. Therefore, the studied organism provides ideal conditions for the comparative analysis of neuroanatomical imaging techniques and the effect of preceding sample preparations of nervous tissue.

We found that wet scanning of whole animals, conducted with μCT turned out to be the least disruptive method. However, in an additional experiment it was discovered that fixation in Bouin's solution, required for μCT scans, resulted in an average tissue shrinkage of 24 % compared to freshly dissected and unfixed brains. The complete sample preparation using fixation in half-strength Karnovsky's solution of dissected brains led to an additional volume decrease of 12.5 %, whereas the preparation using zinc-formaldehyde as fixative resulted in a shrinkage of 5 % in comparison to the volumes obtained by μCT. By minimizing individual variability, at least for aquatic arthropods, this pioneer study aims for the inference of method-based conversion factors in the future, providing a valuable tool for reducing quantitative neuroanatomical data already published to a common denominator. However, volumetric deviations could be shown for all experimental protocols due to methodological noise and/or phenotypic plasticity among genetically identical individuals.

Micro-computed X-ray microscopy using undried tissue is an appropriate non-disruptive technique for allometry of arthropod brains since spatial organ relationships are conserved and tissue shrinkage is minimized. Collecting tissue-based shrinkage factors according to specific sample preparations might allow a better comparability of volumetric data from the literature, even if another technique was applied.

Introduction

55   Micro-computed X-ray tomography and three-dimensional reconstruction of internal

56   morphological structures have opened up new possibilities for analyzing the anatomy of nervous

57   systems in intact specimens (reviewed in Metscher, 2009; Sombke et al., 2015). In addition to

58   vertebrates, the application of X-ray microscopy of soft tissues has been demonstrated to be

59   useful for a variety of metazoan taxa, such as cnidarians (e.g. Holst et al., 2016), nematomorphs

60   (Henne et al., 2016), nematodes (O'Sullivan et al., 2017), polychaetes (e.g. Dinley et al., 2010;

61   Faulwetter et al., 2013), mollusks (e.g. Handschuh et al., 2013), as well as arthropods (e.g.

62   Akkari et al., 2015; Michalik et al., 2013; Sombke et al., 2015; Steinhoff et al., 2017).

63   Whole-mount scanning using confocal laser-scanning microscopy (Krieger et al., 2015; Ott &

64   Elphick, 2003; Ott, 2008) and especially micro-computed X-ray microscopy are suitable

65   methods for precisely capturing three-dimensional structures without the need of histological

66   sections. In samples with various tissue structures densely packed together, most imaging

67   techniques require elaborate contrasting- or staining procedures (Metscher, 2009). In most cases,

68   the tissue must be fixed and dehydrated in advance. The fixation process ideally fulfills the

69   function of counteracting the structural and morphological changes induced by decay, which

70   begins immediately after death of an organism (Lang, 2013). The chosen fixative and its time of

71   penetration, subsequent preparation and imaging technique crucially influence the preservation

72   of the tissue's spatial morphology on which the accuracy of allometric analysis essentially

73   depends. Ethanolic and aldehydic solutions containing formaldehyde (or its polymer

74   paraformaldehyde) or glutaraldehyde are the most widely used chemical fixatives in histology.

75   Aldehydic fixatives protect proteins against denaturation by cross-linking them. No fixative

76   preserves all structures alike, thus usually mixtures are applied (e.g. Bouin or Karnovsky) to

77   compensate adverse effects of single components. Obviously, the preparation should aim to

78   maintain an isotonic milieu for tissue preservation (reviewed in Lang, 2013). For micro-

79   computed X-ray microscopy, contrast-enhancing, especially for the visualization of soft tissues

80   (Gignac et al., 2016; Holst et al., 2016; Metscher, 2009; Mizutani & Suzuki, 2012), is usually

81   realized by increasing adsorption of X-rays applying solutions containing iodine (I_2), osmium

82   tetroxide (OsO_4), or phosphotungstic acid ($H_3PW_{12}O_{40}$) as was demonstrated by Metscher

83   (2009). The sample manipulation in preparation for tomographic imaging for both confocal

84   laser-scanning microscopy as well as micro-computed X-ray microscopy, generally increases the

85   vulnerability to artifacts (Buytaert et al., 2014). Shrinkage artifacts, due to chemical treatment

86   (Lang, 2013) or the scanning itself (Gianoncelli et al., 2015), are very common and apart from
87   mechanical distortions (e.g. caused by bruises and cracks), cannot be fully eliminated even with
88   careful handling (Buytaert et al., 2014). Furthermore, artifacts induced by radiation or chemicals
89   might be occasionally neglected or greatly underestimated in comparative scientific reviews,
90   which might lead to erroneous interpretations.

91   Since more than one hundred years, neuroanatomists always aspired to make their findings
92   quantifiable by inventing more and more ingenious morphometric and allometric methods (see
93   e.g. Hanström, 1926; Snell, 1891). For a meaningful interspecific comparison, quantitative data
94   referring to method-specific artifacts could serve as rewarding tool. Increasing availability of
95   neuroanatomical volumetric data, collected by the use of different methodological approaches of
96   various arthropods (Beltz et al., 2003; Grabe et al., 2015; Hanström, 1926; Schmidt, 2016;
97   Sombke et al., 2015; Tuchina et al., 2015), raises demand for standardizing these data *a*
98   *posteriori*, which constitutes the emphasis of this study. For this purpose, three different well-
99   established sample preparations including two tomographic imaging techniques (confocal laser-
100 scanning microscopy and micro-computed X-ray microscopy) were performed on *P. fallax* cf.
101 *virginalis*. Well identifiable and quantifiable substructures in the crayfish brain such as the
102 deutocerebral chemosensory neuropil and the (deutocerebral) accessory neuropil served as
103 approximation for volume change of tissues. The parthenogenetic marbled crayfish *Procambarus*
104 *fallax* forma *virginalis* (Martin et al., 2010) provides for a rewarding model organism (review:
105 Harzsch et al., 2015) featuring a textbook example of a "typical" astacid brain. The
106 uncomplicated husbandry and year-round parthenogenetic reproduction of the marbled crayfish
107 enables replicable tests using high sample numbers (review: Vogt, 2011).

108

109   Materials and Methods

110   Nomenclature

111 The neuroanatomical nomenclature used in this manuscript is based on Sandeman et al. (1992)
112 and Richter et al. (2010) with some modifications adopted from Harzsch & Hansson (2008),
113 Kenning and Harzsch (2013), and Loesel et al. (2013). The term "oesophageal connective" and

114   the corresponding abbreviation OC (British English) are maintained here for simplicity. The

115   syncerebral brain mass excluding the lateral protocerebrum and visual neuropils of the eyestalks

116   (see Krieger et al., 2015) is termed "central brain" throughout the text according to Schmidt

117   (2016). Although, sample preparations as well as imaging techniques according to the three

118   protocols used vary in a vast of parameters that influence the resulting volume data, each of the

119   three fixatives (zinc-formaldehyde fixative, Bouin's as well as half-strength Karnovsky's

120   solution) is used as a synonym for the entire protocol throughout the text.

121

Animals

123   The specimens of *P. fallax* cf. *virginalis* used in our study were obtained from a commercial

124   aquarium shop (Aquaristik-Langer GbR, https://aquaristik-langer.de/) and were kept together in a

125   freshwater tank at the facilities of the University of Greifswald. For the experimental design,

126   berried individuals were isolated from a community tank, to ensure that all larvae originated

127   from a single individual, and hence were genetically identical. A total of 24 individuals were

128   harvested for pre-tests directly after the juveniles left the maternal pleopods. At this

129   developmental stage, the average body length (rostrum to pleon) measured about 5 mm and the

130   juveniles started autonomous feeding. Morphometric measurements were performed on dead and

131   undissected juveniles in order to ensure that individuals were of the same size. Morphometric

132   analysis was conducted using a Nikon eclipse 90i microscope connected to a Nikon camera DS2-

133   MBWc. For each specimen carapace length and eyestalk width were measured by using the

134   software NIS-Elements AR 3.0. Application of the Shapiro-Wilk-test using the statistical

135   software R 3.2.3 showed normal distribution for carapace length (p = 0.8688) and eyestalk width

136   (p = 0.3054) among the samples. Subsequently, Welch's Two Sample t-test assured that there

137   was no significant difference in measured morphological characters between samples used for

138   confocal laser-scanning microscopy (cLSM) and micro-computed X-ray microscopy (µCT)

139   analysis (carapace length, p = 0.1925 ; eyestalk width, p = 0.1034). Furthermore, six adult

140   animals of different sizes were kindly provided by Gerhard Scholtz (Humboldt University,

141   Berlin, Germany) and kept as described above. These six specimens were used to trace

142   individual volumetric changes in three stages during sample preparation for µCT. Since the

143   scanning of freshly dissected brains without adding any contrast-enhancing agent turned out to

144   be quite challenging, this approach required the use of larger brains (approximately 170 times

145   larger than those of juveniles). Given that the number of specimens is comparably low as well as

146   we assume that the cytochemical compound of adult brains might differ from that of the juvenile

147   brain (e.g. regarding the content of lipids and proteins), the resulting shrinkage factors have to be

148   interpreted with caution.

149

150   **General sample preparation**

151   Genetically identical juveniles of *Procambarus fallax* cf. *virginalis* from the same hatch were

152   taken out of separate tanks with plastic pipettes. They were anaesthetized by chilling them at -18

153   °C in a beaker with little water for a few minutes. Then, the anaesthetized animals were killed by

154   transferring them into watch glasses containing 4 % paraformaldehyde (PFA) and phosphate

155   buffered saline (PBS, pH 7.4; 0.1 M) for 30 minutes at room temperature (RT) on the shaker.

156   After that, PFA was removed by immersing the dead specimens at RT on the shaker for two

157   times (5 min each) in fresh PBS for fixation in half-strength Karnovsky's as well as Bouin's

158   solution, or in HEPES-buffered saline (HBS) for fixation in zinc-formaldehyde (ZnFA) before

159   fixation or brain dissection took place. The procedure of anaesthetization and killing of decapod

160   crustaceans is in concordance with the Animal and Welfare Scientific Panel (AHAW) of the

161   European Food Safety Authority (EFSA) from 2005.

162

163   **Sample preparation for μCT**

164   Before μCT-scanning, seven juvenile siblings were transferred into Eppendorf tubes and

165   immersed in Bouin's solution (10 % formaldehyde, 5 % glacial acetic acid in saturated aqueous

166   picrinic acid). Fixation took place for one week in a fridge (4 °C). After fixation, the animals

167   were gradually dehydrated in ethanol at RT (30 %, 50 %, 60 %, 70 %, 80 %, 90 %, 96 %, and 3 x

168   in 99.5 % ethanol) for 30 min for each step. For enhancing the contrast, samples were incubated

169   in iodine solution (2 % iodine resublimated [Carl Roth GmbH 1 Co. KG, Karlsruhe, Germany;

170   cat. #X864.1] in 99.5 % ethanol) for 24 h in the fridge. Iodine was subsequently washed out of

171   the samples for 5 × 3 min with ethanol. Wet specimens were scanned in a glue sealed pipette tip

172   filled with 99.5 % ethanol (according to Sombke et al., 2015).

173

174   **µCT-Scanning**

175   The scans were performed with a laboratory scaled X-ray-microscope (Xradia MicroXCT-200;

176   Carl Zeiss Microscopy GmbH) entailing geometric and optical magnification. The Bouin-fixed

177   samples of *P. fallax* cf. *virginalis* were scanned with a 20× objective in 99.5 % ethanol with a

178   voltage of 40 kV, a current of 200 µA, and an exposure time of 8 seconds. For all scans, binning

179   2 was applied (summarizing 4 pixels for noise reduction). Projections obtained by the

180   tomography were reconstructed using the software XMReconstructor (Carl Zeiss Microscopy

181   GmbH). To avoid consequent information loss, binning 1 (full resolution) was applied for the

182   following reconstruction resulting in image stacks of 993 × 993 pixels and a pixel size of about

183   1.1 µm. All original image stacks are openly available (see section "data processing") for

184   scientific reproducibility (Davies et al., 2017).

185   For the inference of an individual *in vivo* volume during µCT sample preparation and the

186   comparison of chemically-induced effects on the brain volume, brains were dissected, under tap

187   water at RT from a total of another six adult animals of different sizes, and each was

188   immediately scanned (stage 1) moistly within a sealed Eppendorf tube at 20 kV and 3 W for 1

189   sec (binning 4) with 400 projections reducing the total scan time to 15 min. Brains were

190   subsequently fixed in Bouin's solution overnight in the fridge. Bouin's solution was replaced two

191   times by tap water and the brain was immediately scanned (stage 2) again moistly using the

192   identic scanning parameters. Afterwards, these fixed brains were gradually dehydrated as

193   outlined above in addition with contrast enhancement by dissolved iodine (2 %) in ethanol before

194   being scanned a third time (stage 3) in 99.5 % ethanol using again the same scanning parameters.

195

196   **Sample preparation for cLSM**

197   **Fixation in half-strength Karnovsky's solution for enhancing autofluorescence of nervous**

198   **tissue**

199   The two pairs of antennae as well as the eyestalks were removed and the brains of a total of six

200   specimens were dissected in PBS (0.1 M; pH 7.4) using precision forceps (DUMONT®; type

201   55). The brains were fixed in half-strength Karnovsky's fixative, a mixture of 2 %

202   glutaraldehyde [Electron Microscopy Sciences, 1560 Industry Road, USA-Hatfield, PA 19440;

203   Cat-No. 16220] and 2 % PFA [Carl Roth GmbH 1 Co. KG, Karlsruhe, Germany; Cat-no. 0335.2]

204   in PBS (0.1 M; pH 7.4) for a week at 4 °C. Subsequently, a gradual dehydration of the samples

205   was conducted in ethanol (50 %, 70 %, 80 %, 90 % for 10 min each, 96 % for 30 min, and in

206   99.5 % ethanol for 2 x 30 min) at RT.

207

208   **Fixation in zinc-formaldehyde and immunhistochemical labeling**

209   The whole mount labeling protocol after Ott (2008) was applied to improve antibody penetration

210   into nervous tissues, as compared to traditional PFA-fixation. For this method, a total of seven

211   animals were killed by a few drops of formalin instead of 4 % PFA in PBS to avoid precipitation

212   of zinc phosphate in combination with ZnFA in the following steps (compare Ott, 2008). The

213   central brain was then dissected in HBS as described before and fixed in 4 % ZnFA (Electron

214   Microscopy Sciences, 1560 Industry Road, USA-Hatfield, PA 19440; Cat-No. 15675) on a

215   shaker for 20 h at RT. The fixed brains were subsequently washed for 3 x 15 min in HBS, and

216   instantly dehydrated and postfixed in DENT's fixative (20 % DMSO [Serva Electrophoresis,

217   Heidelberg, Germany; Cat-No. 20385] / 80 % methanol) in a drop of HBS on the shaker again

218   for 2 h, at RT. Afterwards, the brains were transferred into 99 % methanol. The samples were

219   gradually rehydrated in TRIS-buffer with varying grades of methanol (90 %, 70 %, 50 %, 30 %

220   methanol, and finally, pure TRIS-buffer for 15 min each). Samples were preincubated for 2 x 2 h

221   in PBS-TX (0.3 % triton, 0.02 % sodium azide, 1 % bovine serumalbumin [BSA]) at RT,

222   followed by incubation in monoclonal mouse anti-synapsin antibody (3C11 anti SYNORF1;

223   Developmental Studies Hybridoma Bank, University of Iowa; deposited by E. Buchner,

224   University Hospital Würzburg, Germany; diluted 1:1 in glycerol) in PBS (1:1000) for 4 days at 4

225   °C. Excess primary antibody was washed in PBS-TX for 4 x 30 min at RT. Incubation of the Cy

226   3-conjugated secondary antibody (goat anti-mouse; Jackson Immuno Research; 1:1 in glycerol)

227   in HBS (1:500) was carried out in the fridge (4 °C) for 2.5 days. After washing for 2 x 1 h in

228   PBS-TX, the samples were dehydrated in ethanolic solutions of different grades (30 %, 50 %, 70

229 %, 80 %, 90 %, 96 %, and 99.5 % for 30 min each) at RT. Regarding antibody specificity, has

230 been shown that the monoclonal mouse-anti-*Drosophila* antibody 3C11 consistently labels

231 synaptic brain regions in representatives of all major subgroups of the malacostracan crustaceans

232 (see Beltz et al., 2003; Harzsch & Hansson, 2008; Harzsch et al., 1997, 1999, Krieger et al.,

233 2012, 2015; Meth et al., 2017; Vilpoux et al., 2006). Hence, it can be assumed that this antibody

234 does in fact label synaptic neuropils in Malacostraca (for more details see Krieger et al., 2015).

235 **cLSM-scanning**

236 Scanning was conducted on a confocal laser-scanning microscope (Leica TCS SP5 II). For

237 optimal light transmission, tissues were cleared in 98 % methyl salicylate (Merck, Darmstadt,

238 Germany; Cat-no. W274518). After dehydration in ethanol, brains that were previously fixed in

239 ZnFA (n=7) as well as in half-strength Karnovsky's solution (n=6) were transferred into custom-

240 made scan chambers filled with pure methyl salicylate before confocal laser-scanning. Scanning

241 was performed with an inverted Leica TCS SP5II (Leica, Wetzlar, Germany) using a DPSS-laser

242 with an excitation wavelength of 561 nm and a speed of 400 Hz. For detection of fluorescence

243 (emitted by glutaraldehyde-enhanced autofluorescence as well as by Cy3-conjugates of the

244 secondary antibody), a 10 x objective with a numerical aperture of 0.4 was used resulting in

245 stacked images of 1024 x 1024 pixels with a pixel size of about 0.8 μm. The confocal

246 microscope operated with a pinhole size of 53 μm in diameter and in steps of 1.33 μm (system-

247 optimized to 1 airy unit and refractive correction for aqueous immersion media).

248

249 **Data processing**

250 Volume reconstruction and visualization was carried out using Amira 5.6.0. (FEI Visualization

251 Science Group, Burlington, USA). The central brain, the deutocerebral chemosensory lobes

252 (DCLs) as well as the accessory lobes (AcNs) were segmented manually for volumetric analysis.

253 Three-dimensional surfaces corresponding to the segmentation were generated using

254 unconstrained smoothing (Amira: SurfaceGen). Voxel data of the reconstructed neuropils were

255 extracted by using Amira`s material statistics tool. The outline of scans of dissected brains could

256 be instantly visualized without further virtual segmentation by using the Amira Isosurface-

257 module. Morphological deformations based on anisometric shrinkages could be detected this
258 way.

259 Raw data of brain section series (based on µCT as well as cLSM) is available from
260 https://www.morphdbase.de (Grobe & Vogt, 2009) under the "media" tab under "Krieger". A
261 combination of the short title "Nischik and Krieger (2017) Marmorkrebs", an identifier
262 according to the specimen, and an abbreviation for the method applied (e.g. Nischik and Krieger
263 (2017) Marmorkrebs01_µCT) is given for each of the 20 image stacks in addition to 18 image
264 stacks of brains of another six adult specimens which were scanned 1) freshly dissected prior to
265 fixation; 2) fixed with Bouin's solution overnight but without any dehydration as well as any
266 contrast agent; and 3) after fixation, dehydration in ethanol, and contrast enhancement using 2%
267 iodine. Please note that due to technical requirements of MorphDBase ver. 3.3, all µCT-datasets
268 had to be reduced in color depth from 16 bit to 8 bit prior to uploading. In contrast to the datasets
269 from µCT-scanning, all cLSM-based datasets feature anisotropic voxels. The original voxel-size
270 is lost due to a conversion of the file format prior to uploading. For displaying these image stacks
271 in the correct spatial relationship, the voxel-size has to be resized for each image stack according
272 to the voxel dimensions given in table 1 (including the correction factor to minimize refractive
273 mismatch from Bucher et al. (2000) of 1.581 in the z-axis).

274 Furthermore, table 2 summarizes the volumes of the central brain, of the DCLs, and AcNs of
275 both brain hemispheres according to the three methods applied as well as the z-corrected
276 volumes due to a putative refractive mismatch in cLSM-scans. In table 3, the volumes of the
277 central brain of six adult specimens are summarized which were analyzed for evaluation of tissue
278 shrinkage throughout the sample preparation (stages 1 to 3) prior to µCT-scanning of fixed and
279 contrast-enhanced samples.

280

281 **Statistics**

282 The acquired volume data (Fig. 1) were exported into Microsoft® Excel for descriptive statistics.
283 Statistical analyses were performed with the "stats"-package and illustrated with the "graphics"-
284 package of R 3.2.3. A one-way analysis of variance (ANOVA) was carried out for calculation of
285 statistical significant differences between volumetric data and the methods used (Fig. 2). The

286   effects of treatment on the volume of the subunits DCLs and AcNs, as well as on the total

287   volume of the central brain were calculated for each structure by Tukey's post-hoc test. A paired

288   two sample Student's t-test was applied for volumes of left and right lobe of AcN and DCL

289   respectively, to test reproducibility of the manual volume reconstruction, which was conducted

290   by the same investigator for each specimen. A Wilcoxon signed rank test was applied to test the

291   effect of chemically induced difference in the brain volume throughout the sample preparation

292   for μCT-scanning.

293

294   **Results**

295   **μCT**

296   Tomograms were generated with μCT to morphometrically analyze the brain of *P. fallax* cf.

297   *virginalis*. Volume rendering allowed virtually sectioning of the animal in different planes for

298   neuroanatomical analysis as well as visualizing the brain in its natural position within the

299   cephalon (Figs. 3A to D). The image contrast as a function of the tissue density was high enough

300   to allow identification of single neuropils (compare Figs. 4A and B). Thus, the central brain

301   including the DCLs and the AcNs could be reconstructed (Figs. 3C and D). The central brain is

302   vertically curved and held in its upright position by the protocerebral tract originating in the

303   lateral protocerebrum (latPC; Figs. 3C and D) within the eyestalks as well as by the nerves of the

304   antennae 1 and 2 (A_I and A_{II}; Figs. 3A and C). Here, an approximate *in situ* coherent

305   reconstruction of the neuropils in their spatial context is assumed, since only a few steps of

306   sample preparation were required for scanning an animal as a whole.

307

308   While μCT-scanning of contrasted tissues delivered a high image contrast, the analysis of μCT-

309   scans of unfixed as well as fixed brains (without any contrast agent) of another six adult

310   specimens, which were used for inferring individual *in vivo* volumes during μCT sample

311   preparation, turned out to be fairly challenging. In freshly dissected as well as in Bouin-fixed but

312   uncontrasted brains, the image contrast was barely high enough to identify the limits of the tissue

313   surfaces but did not suffice to identify internal substructures such as neuropils or cell clusters.

314   Therefore, the use of larger brains of adult specimens (approximately 170 times larger than those

315   of juveniles) was essential. The central brain volume resulted in a significant average shrinkage

316   of 24 % (ranging from 7.9 to 44.8 %) after fixation in Bouin's solution (Wilcoxon signed rank

317   test: p = 0.0313; n = 6) and no further significant shrinkage (Wilcoxon signed rank test: p =

318   0.6875; n = 6) after dehydration and contrast-enhancement using 2 % iodine in ethanol (Fig. 5

319   and table 3).

320

321

322   **cLSM**

323   **Autofluorescence in** half-strength **Karnovsky's solution**

324   Tissues fixed with half-strength Karnovsky's solution resulted in cLSM scans characterized by a

325   high resolution and remarkable signal to noise ratio. Furthermore, intricate histological details

326   such as individual olfactory glomeruli in the DCL and even microglomeruli within the AcN were

327   resolved with high accuracy (compare Figs. 4A and C).

328

329   **Immunhistochemistry, ZnFA-Fixation**

330   In comparison to the previously described method, volume divergences may only be the result of

331   the fixation of the specimen – in this case using the ZnFA-fixation protocol after Ott (2008) and,

332   of course, of the individual bias, due to manual segmentation for three-dimensional

333   reconstruction in Amira. In fact, the reconstructed volumes differ only slightly, and thus, no

334   statistically significant difference between the applied fixations (ZnFA and half-strength

335   Karnovsky's solution) could be detected for each of the brain substructures analyzed (Fig. 2).

336   However, a slightly higher average volume indicates, that the whole brain is somewhat better

337   preserved by using the fixation with ZnFA and dehydrogenation in methanol and DMSO. Since

338   an immunohistochemical labeling was used here, the resulting tissue contrast is different to that

339   of autofluorescence in half-strength Karnovsky's solution (compare Figs. 4C and D). In this case,

340   primarily areas in which the synaptic membrane protein synapsin was present were stained (Fig.

341   4D). While the intention was to facilitate the identification of neuropil regions, it actually

342   increased image noise.

343

344   **µCT *versus* cLSM**

345   All three methods very likely differ to a certain degree from *in vivo* congruent nervous tissue

346   volume. Since all samples at least temporarily were exposed to hyperosmolar media resulting in

347   dehydration, it has to be assumed that artifacts due to shrinkage most likely occurred. An

348   expansion of the tissue seems unlikely, since also in the wet-scan µCT approach, dehydration

349   takes place (e.g. fixation in Bouin's solution, dehydration in ethanol). However, neither the

350   general imaging technique (µCT *vs*. cLSM: Welch's Two Sample t-test: p = 0.2136; n = 20), nor

351   the choice of fixative between both cLSM approaches did influence the tissue volumes

352   significantly (Welch's Two Sample t-test: p = 0.4541; n = 13). Assuming a symmetrical

353   development of both brain hemispheres, the investigator's individual bias in manual

354   segmentation for three-dimensional reconstruction was tested by comparing volumes of both

355   hemispheres. While the volume of the accessory lobes reliably exceeded the volume of the

356   deutocerebral chemosensory lobes (single-factor ANOVA: p < 0.001; n = 20), no difference in

357   the volume of the left and right hemispheres of paired lobes could be found in any given

358   treatment (paired Student's t-test: DCL: p = 0.2691; AcN: p = 0.1107; n = 20).

359

360   The highest DCLs-volumes (total volume of both hemispheres) were reconstructed in specimens

361   which were fixed in Bouin's solution and imaged by the use of µCT (mean DCLs volume [mm^3]:

362   0.0029 ± 0.0003; n = 7). The DCLs volumes in specimens fixed in ZnFA (mean DCLs volume

363   [mm^3]: 0.0027 ± 0.0006; n = 7) were insignificantly higher compared to specimens fixed in half-

364   strength Karnovsky's solution (mean DCLs volume [mm^3]: 0.0025 ± 0.0003; n = 6). The

365   measured volume of nervous tissue was most congruent to assumed *in vivo* volume when

366   specimens were fixed in Bouin and scanned in ethanol with µCT (Figs 1, 2, and 5). This is

367   followed by cLSM visualization of whole-mounts fixed in ZnFA and at last of tissues fixed in

368   half-strength Karnovsky's solution (compare Figs. 1A, B, and C). Although µCT derived

369   volumes are significantly smaller than those of freshly dissected brains (average of 24 %,

370   ranging from 7.9 to 44.8 %), cLSM tomograms of tissues fixed in half-strength Karnovsky's

371   solution reveal a further relative shrinkage of 12.5 %; and of 5 % when using ZnFA-fixation.

372

373   In *P. fallax* cf. *virginalis*, light-microscopic imaging techniques on the brain require the removal

374   of the cuticle or dissection of the nervous tissue, thus an analysis of the brain within the animal is

375   only feasible by using x-ray -or magnetic resonance imaging techniques (Brinkley et al., 2005;

376   Herberholz et al., 2004; Köhnk et al., 2017, and reviewed in Ziegler et al., 2011). Three-

377   dimensional surfaces of half-strength Karnovsky's solution-fixed brains, based on isosurfaces

378   using a grayscale-threshold (Amira: Isosurface), appeared more porous and wrinkled (compare

379   Figs. 6A to C), while the ZnFA-fixed brains had a smoother appearance (compare Figs. 6D to F).

380   Along the neuraxis, brains appear more furrowed after fixation with half-strength Karnovsky's

381   solution compared to those fixed with ZnFA (Figure 6). In addition, the bilaterally symmetric

382   antenna-2-nerve ($A_{II}Nv$; Figs. 6D and F) was better preserved in its fibrous organization in ZnFA

383   preparations compared to those fixed with half-strength Karnovsky's solution (Figs. 6A and C).

384   For comparison of image quality, a schematic overview of the central brain (Fig. 4A) as well as

385   virtual frontal sections recorded on a similar anatomical plane (approximately as shown in Fig.

386   3B) are shown in Figure 4B to D. In images generated by cLSM within the DCL, individual

387   olfactory glomeruli are visible (Figs. 4C and D). The images produced by µCT have a lower

388   resolution and a lower signal-to-noise ratio. Here, the identification of individual olfactory

389   glomeruli at least at the chosen magnification is not possible (Figure 4B). In fact, the highest

390   contrast was obtained by confocal imaging of half-strength Karnovsky's solution-fixed tissue

391   (Fig. 4C). By the use of autofluorescent enhancement of half-strength Karnovsky's solution-

392   fixation, the sample preparation is much less time consuming but more unspecific than applying

393   the two-step protocol of immunhistochemical labeling. The high resolution in both methods

394   reveals details like individual olfactory glomeruli of the DCLs as well as even microglomeruli

395   within the AcNs (Figs. 4A, C, and D).

396

397   **Discussion**

398   Confocal laser-scanning microscopy turned out to be the most suitable technique for

399   identification of neuropils and neuronal somata (Figs. 4A, C, and D). Nevertheless, for the use of

400   brain morphometry at a coarse level, the image contrast is sufficient to distinguish the neuropils

401   from the surrounding tissue in all applied techniques. In contrast to the preparation for µCT, the

402   central brain has to be dissected for cLSM whole mounts, which comes with some

403   disadvantages. The process of sample preparation alters the brain's characteristic shape, which

404   *in-situ* is displaying a curvature along the neuraxis. Due to dissection, the originally upstanding

405   central brain collapses so that spatial relationships of brain regions become artificial. In addition,

406   the use of methyl salicylate for clearing in advance of cLSM-scanning has been reported to cause

407   unpredictable shrinkage of nervous tissues ranging from 3.5 to 27 % of the volume (Bucher et

408   al., 2000). Furthermore, a refractive mismatch along the z-axis must be considered for the use of

409   methyl salicylate as mounting medium for cLSM whichleads to enormous aberrations of volume

410   (Bucher et al., 2000). Using the z-axial correction factor to eliminate refractive mismatch for the

411   use of methyl salicylate provided by Bucher et al. (2000) of 1.581 (for a 10x dry objective with a

412   numerical aperture of 0.40) resulted in spatial congruence of the brain dimensions that almost

413   equals those based on μCT-scans. The resulting volumes of brains fixed in ZnFA as well as in

414   half-strength Karnovsky's solution were still insignificantly smaller (ZnFA *vs*. Bouin: 5 %; p =

415   0.826; half-strength Karnovsky's solution *vs*. Bouin: 12.5 %; p = 0.362; one-way ANOVA) than

416   those obtained from μCT-scans. The refractive mismatch is often altered bythe anisometric

417   distribution of clearing agent, different refractive indices of the tissues analyzed and thus, its

418   progression along the z-axis is not linear (Hell et al., 1993; Besseling, Jose & Blaaderen, 2015).

419   The anisometry of cLSM-stacks as a result of optical limitations and the associated necessity of a

420   z-axial correction factor prior to analysis hence adds another source of inaccuracy compared to

421   μCT-datasets. Although, brain volumes based on cLSM-stacks that were axially rescaled are

422   insignificantly smaller, the sample preparation seems to have a higher influence on tissue

423   shrinkage than the sample preparation for μCT-scanning. Also, the accuracy of volumetric

424   analysis is decreased when using the fixation of ZnFA in addition with immunohistochemical

425   labeling against synapsins compared to the sample preparations using Bouin and half-strength

426   Karnovsky's solution, resulting in higher variances. One explanation could be that since the

427   latter two approaches (using Bouin as well as half-strength Karnofsky's solution) are based on

428   the detection of differences in tissue densities, the sample preparation using ZnFA is basically

429   dependent on the cross-linking of the antibody against SYNORF1, and thus the distribution of

430   the target epitopes.

431

432   While volumetry can be helpful to analyze differences in the size relation of brain structures

433   within an organism, as well as for interspecific comparison, referring brain size as a function of

434   cognitive capacity, is highly debated (Chittka & Niven, 2009; Healy & Rowe, 2013). However,

435   for example in honeybees (Durst et al., 1994; Groh et al., 2006) or in leaf-cutting ants (Groh et

436   al., 2014), morphometric analysis showed an age and experience dependent difference in

437   neuropil volume of the mushroom body. Especially for the volumetry of these tiny brain

438 subcompartments, measurement errors can have a huge impact and should therefore be

439 minimized. It is therefore important to consider the osmolality of immersive chemicals (fixatives

440 and buffers) in respect to the target tissue. Increased tissue shrinkage was reported with

441 increasing hypertonia (Rasmussen, 1974), hence chemical fixatives with similar osmolality as

442 the original osmotic environment (e.g. < 280 mOsm/kg H_2O for freshwater species) are

443 recommended (Bullock, 1984; Coetzee & van der Merwe, 1985). An area shrinkage of 11 - 20 %

444 was reported for rabbit corneal endothelial cells fixed with Karnovsky fixative (850 mOsM/kg;

445 Doughty et al., 1997). However, in the current study merely a half-strength Karnovsky fixative

446 (640 mOsM/kg; Platt et al., 1997) was applied. Ott (2008) described a new fixation protocol for

447 immunhistochemical staining, which uses ZnFA instead of PFA resulting in lower osmolality

448 (325 mOsm/kg). This has been shown to improve antibody penetration and preservation of

449 spatial brain morphology. Ott (2008) demonstrated effects of different fixation protocols on

450 morphological preservation on the brain of the desert locust *Schistocerca gregaria*. Ott showed

451 that fixation using PFA lead to increased wrinkling in contrast to ZnFA-fixation. Likewise, the

452 nature of dehydration and the duration of fixation were found to be decisive factors. This

453 corresponds to findings from Ott (2008), as preparations with a shorter fixing time in ZnFA

454 showed a lower wrinkling. Here, the cLSM-tomograms resulted in smoother surfaces of brains

455 analyzed.

456 Apart from indirect volumetric measurements evaluated here, a possible approach to obtain

457 approximate *in vivo* volumes for invertebrate brains, would be the use of a micro-volumeter

458 according to Douglass and Wcislo (2010), as an example for direct volumetry. By the use of

459 Archimedes' principle, the dissected brain is put in a liquid-filled tube and the occurring volume

460 displacement of the liquid can be measured with a micro-pipette stepwise until the previous

461 meniscus is reached. In this way, the total removed volume equals the actual brain volume.

462 However, based on initial trials, instrumental errors still outweigh a precise measurement of very

463 small volumes (< 1 ml). This technique needs more precise adjustment for readout of the

464 meniscus. A successful application of direct volumetry using Archimede's principle or high

465 resolution magnetic resonance imaging of living animals will offer a conclusive reference for *in*

466 *vivo* brain volumes. Although the sample size is not markedly high (n = ranging from 6 to 7 per

467 treatment), we consider that specimens prepared for µCT feature the closest *in vivo* coherence

468 (24 % average shrinkage; ranging from 7.9 to 44.8 %). We could show that shrinkage due to

469   each single step throughout the sample preparation was primarily influenced by the fixation in

470   Bouin, whereas the subsequent steps of this preparation interestingly did not contribute

471   substantially to tissue shrinkage. However, dehydration in ethanol in addition with contrast-

472   enhancement by iodine (Buytaert et al., 2014) as well as the scanning procedure itself

473   (Gianoncelli et al., 2015) indeed most likely lead to a deviation from the *in vivo* volume.

474   The deutocerebral chemosensory and accessory lobes are convenient landmarks for a volumetric

475   evaluation of experimental effects, due to their conspicuous structure with an almost spherical

476   shape, they can be easily identified. Especially for the conspicuous deutocerebral chemosensory

477   lobes, volumetric data are available for a considerable number of crustacean species (see Beltz et

478   al., 2003; Krieger et al., 2015; Tuchina et al., 2015; and review in Schmidt, 2016). In particular,

479   the relative volumes of these homologous brain regions vary greatly among species. For

480   comparison, table 4 displays the volume information for the deutocerebral chemosensory lobes

481   of selected crustacean species accompanied by the data obtained for *P. fallax* cf. *virginalis*.

482   However, it should be noted that all individuals of *P. fallax* cf. *virginalis* analyzed for the

483   comparison of imaging techniques were juvenile siblings with a body length of about 5 mm.

484   Adults of this species can reach a body length of 120 mm, and thus feature markedly larger brain

485   sizes (ranging up to 300 times higher volumes than those of the juveniles analyzed here).

486   Furthermore, it can be expected that methods including chemicals do not influence volumes of

487   different brain substructures alike (such as somata or fibers). Since the main volume of the brain

488   is dominated by neuropils as well as the fact that all three methodological approaches did not

489   meet the requirements of a differentiated volumetric analysis, an inhomogeneous tissue

490   shrinkage was neglected for simplicity.

491   For interspecific comparisons and the corresponding phylogenetic or neuroanatomical value of

492   volumetric data, several factors have to be standardized, such as the experimental procedure

493   including fixatives and technique of volumetry (e.g. histological sections with volumetric

494   extrapolations based on the section thickness, or 3D-reconstruction of tomographic data).

495   Shrinkage factors, based on the morphometric method and fixatives used, can serve as a tool to

496   approximate already referred volumetric data to a common denominator for a more reasonable

497   interspecific comparison. Because of its parthenogenetic nature, *P. fallax* cf. *virginalis* is well

498   suited generating such a reference system at least for aquatic arthropods featuring a comparable

499 osmolality. Although the juvenile specimens analyzed were genetically identical and of the same

500 age (clutch), individual brain sizes might vary due to phenotypic plasticity as has been shown

501 e.g. for the marmoration pattern in siblings of the Marmorkrebs (review: Vogt, 2011), but also

502 for brain sizes in clones of *Daphnia magna* (Macagno et al., 1973), and also in vertebrates

503 (review: Mitchell, 2007). Consequently, comparative brain allometry in juvenile isogenetic

504 siblings appears to be the most favorable approximation to neglect inter-individual variations.

505

506

507 **Conclusions**

508 Although today, neuroanatomical volumetric data are available for a variety of crustacean

509 species, interspecific comparisons often suffer from methodological differences in volumetry.

510 Variations in tissue volume as artefacts of experimental sample preparation, such as fixation

511 procedures, might be incorrectly assigned to biological phenomena. While comparative brain

512 morphometry and especially volumetry as a measure for cognitive capabilities is controversially

513 discussed (Chittka & Niven, 2009; Healy & Rowe, 2013), it is, however, a useful tool for other

514 fields of interest, such as the neural development (Helluy et al., 1995), neurophylogeny as well

515 as specific evolutionary adaptations of the nervous system (Beltz et al., 2003; Krieger et al.,

516 2015; reviewed in Schmidt, 2016). Therefore, a standardization of method-based deviations is

517 highly recommended. Here, we aimed at a consistent methodological approach to evaluate

518 standard imaging techniques as well as to obtain conversion factors to deduce approximate *in*

519 *vivo* volumes based on the method of analysis. Well-founded conversion factors will allow for *a*

520 *posteriori* standardization of determined nervous tissue volumes in malacostracans, and therefore

521 help to eliminate the aforementioned sources of error. Due to its parthenogenetic reproduction, *P.*

522 *fallax* cf. *virginalis* produces genetically identical offspring making it an ideal model organism

523 especially for methodological studies. Further comparative studies covering all standard

524 techniques in the same manner, will offer a conclusive reference system and comparability,

525 irrespective of fixation protocol chosen which is indeed dependent of the imaging technique and

526 the specific scientific question.

527

Acknowledgements

We cordially thank Gerhard Scholtz (Humboldt-University of Berlin) for the kind provision of
animals and Caroline Viertel (University of Greifswald) for the animal husbandry in the
laboratory. We like to express our gratitude to Steffen Harzsch and Marie K. Hörnig (University
of Greifswald) for reading and improving the manuscript. We would like to thank both
anonymous reviewers for their input, as these recommendations led us to markedly improve the
manuscript.

References

Akkari N., Enghoff H., Metscher BD. 2015. A New Dimension in Documenting New Species:
High-Detail Imaging for Myriapod Taxonomy and First 3D Cybertype of a New
Millipede Species (Diplopoda, Julida, Julidae). *PLOS ONE* 10:e0135243. DOI:
10.1371/journal.pone.0135243.

Beltz BS., Kordas K., Lee MM., Long JB., Benton JL., Sandeman DC. 2003. Ecological,
evolutionary, and functional correlates of sensilla number and glomerular density in the
olfactory system of decapod crustaceans. *The Journal of Comparative Neurology*
455:260–269. DOI: 10.1002/cne.10474.

Besseling TH., Jose J., Blaaderen AV. 2015. Methods to calibrate and scale axial distances in
confocal microscopy as a function of refractive index. *Journal of Microscopy* 257:142–
150. DOI: 10.1111/jmi.12194.

Brinkley CK., Kolodny NH., Kohler SJ., Sandeman DC., Beltz BS. 2005. Magnetic resonance
imaging at 9.4 T as a tool for studying neural anatomy in non-vertebrates. *Journal of
Neuroscience Methods* 146:124–132. DOI: 10.1016/j.jneumeth.2005.02.003.

551   Bucher D., Scholz M., Stetter M., Obermayer K., Pflüger H-J. 2000. Correction methods for

552   three-dimensional reconstructions from confocal images: I. tissue shrinking and axial

553   scaling. *Journal of Neuroscience Methods* 100:135–143. DOI: 10.1016/S0165-

554   0270(00)00245-4.

555   Bullock GR. 1984. The current status of fixation for electron microscopy: A review. *Journal of*

556   *Microscopy* 133:1–15. DOI: 10.1111/j.1365-2818.1984.tb00458.x.

557   Buytaert J., Goyens J., De Greef D., Aerts P., Dirckx J. 2014. Volume shrinkage of bone, brain

558   and muscle tissue in sample preparation for micro-CT and light sheet fluorescence

559   microscopy (LSFM). *Microscopy and Microanalysis* 20:1208–1217. DOI:

560   10.1017/S1431927614001329.

561   Chittka L., Niven J. 2009. Are Bigger Brains Better? *Current Biology* 19:R995–R1008. DOI:

562   10.1016/j.cub.2009.08.023.

563   Coetzee J., van der Merwe CF. 1985. Effect of glutaraldehyde on the osmolarity of the buffer

564   vehicle. *Journal of Microscopy* 138:99–105. DOI: 10.1111/j.1365-2818.1985.tb02602.x.

565   Davies TG., Rahman IA., Lautenschlager S., Cunningham JA., Asher RJ., Barrett PM., Bates

566   KT., Bengtson S., Benson RBJ., Boyer DM., Braga J., Bright JA., Claessens LPAM.,

567   Cox PG., Dong X-P., Evans AR., Falkingham PL., Friedman M., Garwood RJ., Goswami

568   A., Hutchinson JR., Jeffery NS., Johanson Z., Lebrun R., Martínez-Pérez C., Marugán-

569   Lobón J., O'Higgins PM., Metscher B., Orliac M., Rowe TB., Rücklin M., Sánchez-

570   Villagra MR., Shubin NH., Smith SY., Starck JM., Stringer C., Summers AP., Sutton

571   MD., Walsh SA., Weisbecker V., Witmer LM., Wroe S., Yin Z., Rayfield EJ., Donoghue

572   PCJ. 2017. Open data and digital morphology. *Proc. R. Soc. B* 284:20170194. DOI:

573   10.1098/rspb.2017.0194.

574 Dinley J., Hawkins L., Paterson G., Ball A d., Sinclair I., Sinnett-Jones P., Lanham S. 2010.

575   Micro-computed X-ray tomography: a new non-destructive method of assessing

576   sectional, fly-through and 3D imaging of a soft-bodied marine worm. *Journal of*

577   *Microscopy* 238:123–133. DOI: 10.1111/j.1365-2818.2009.03335.x.

578 Doughty MJ., Bergmanson JPG., Blocker Y. 1997. Shrinkage and distortion of the rabbit corneal

579   endothelial cell mosaic caused by a high osmolality glutaraldehyde-formaldehyde

580   fixative compared to glutaraldehyde. *Tissue and Cell* 29:533–547. DOI: 10.1016/S0040-

581   8166(97)80054-7.

582 Douglass J., Wcislo W. 2010. An inexpensive and portable microvolumeter for rapid evaluation

583   of biological samples. *BioTechniques* 49:566–572. DOI: 10.2144/000113464.

584 Durst C., Eichmüller S., Menzel R. 1994. Development and experience lead to increased volume

585   of subcompartments of the honeybee mushroom body. *Behavioral and Neural Biology*

586   62:259–263. DOI: 10.1016/S0163-1047(05)80025-1.

587 Faulwetter S., Vasileiadou A., Kouratoras M., Dailianis T., Arvanitidis C. 2013. Micro-

588   computed tomography: Introducing new dimensions to taxonomy. *ZooKeys* 263:1–45.

589   DOI: 10.3897/zookeys.263.4261.

590 Gianoncelli A., Vaccari L., Kourousias G., Cassese D., Bedolla DE., Kenig S., Storici P.,

591   Lazzarino M., Kiskinova M. 2015. Soft X-Ray Microscopy Radiation Damage On Fixed

592   Cells Investigated With Synchrotron Radiation FTIR Microscopy. *Scientific Reports*

593   5:10250. DOI: 10.1038/srep10250.

594 Gignac PM., Kley NJ., Clarke JA., Colbert MW., Morhardt AC., Cerio D., Cost IN., Cox PG.,

595   Daza JD., Early CM., Echols MS., Henkelman RM., Herdina AN., Holliday CM., Li Z.,

596   Mahlow K., Merchant S., Müller J., Orsbon CP., Paluh DJ., Thies ML., Tsai HP., Witmer

597   LM. 2016. Diffusible iodine-based contrast-enhanced computed tomography (diceCT):

598   an emerging tool for rapid, high-resolution, 3-D imaging of metazoan soft tissues.

599   *Journal of Anatomy* 228:889–909. DOI: 10.1111/joa.12449.

600 Grabe V., Strutz A., Baschwitz A., Hansson BS., Sachse S. 2015. Digital *in vivo* 3D atlas of the

601   antennal lobe of *Drosophila melanogaster*. *Journal of Comparative Neurology* 523:530–

602   544. DOI: 10.1002/cne.23697.

603 Grobe P., Vogt L. 2009. *Morph.D.Base 2.0: A public data base for morphological data,*

604   *metadata, and phylogenetic matrices.*

605 Groh C., Ahrens D., Rössler W. 2006. Environment- and Age-Dependent Plasticity of Synaptic

606   Complexes in the Mushroom Bodies of Honeybee Queens. *Brain, Behavior and*

607   *Evolution* 68:1–14. DOI: 10.1159/000092309.

608 Groh C., Kelber C., Grübel K., Rössler W. 2014. Density of mushroom body synaptic complexes

609   limits intraspecies brain miniaturization in highly polymorphic leaf-cutting ant workers.

610   *Proceedings of the Royal Society of London B: Biological Sciences* 281:20140432. DOI:

611   10.1098/rspb.2014.0432.

612 Handschuh S., Baeumler N., Schwaha T., Ruthensteiner B. 2013. A correlative approach for

613   combining microCT, light and transmission electron microscopy in a single 3D scenario.

614   *Frontiers in Zoology* 10:44. DOI: 10.1186/1742-9994-10-44.

615 Hanström B. 1926. Untersuchungen über die relative Grösse der Gehirnzentren verschiedener

616   Arthropoden unter Berücksichtigung der Lebensweise. *Zeitschrift fur Mikroskopisch-*

617   *Anatomische Forschung* 7:135–190.

618 Harzsch S., Anger K., Dawirs RR. 1997. Immunocytochemical detection of acetylated alpha-

619   tubulin and *Drosophila* synapsin in the embryonic crustacean nervous system. *The*

620   *International Journal of Developmental Biology* 41:477–484.

621 Harzsch S., Hansson BS. 2008. Brain architecture in the terrestrial hermit crab *Coenobita*

622   *clypeatus* (Anomura, Coenobitidae), a crustacean with a good aerial sense of smell. *BMC*

623   *Neuroscience* 9:58. DOI: 10.1186/1471-2202-9-58.

624 Harzsch S., Krieger J., Faulkes Z. 2015. "Crustacea": Decapoda – Astacida. In: Wanninger A ed.

625   *Evolutionary Developmental Biology of Invertebrates 4*. Springer Vienna, 101–151. DOI:

626   10.1007/978-3-7091-1853-5_4.

627 Harzsch S., Miller J., Benton JL., Beltz BS. 1999. From embryo to adult: persistent neurogenesis

628   and apoptotic cell death shape the lobster deutocerebrum. *Journal of Neuroscience*

629   19:3472–3485.

630 Healy SD., Rowe C. 2013. Costs and benefits of evolving a larger brain: doubts over the

631   evidence that large brains lead to better cognition. *Animal Behaviour* 86:e1–e3. DOI:

632   10.1016/j.anbehav.2013.05.017.

633 Hell S., Reiner G., Cremer C., Stelzer EHK. 1993. Aberrations in confocal fluorescence

634   microscopy induced by mismatches in refractive index. *Journal of Microscopy* 169:391–

635   405. DOI: 10.1111/j.1365-2818.1993.tb03315.x.

636 Helluy SM., Ruchhoeft ML., Beltz BS. 1995. Development of the olfactory and accessory lobes

637   in the american lobster: An allometric analysis and its implications for the deutocerebral

638   structure of decapods. *The Journal of Comparative Neurology* 357:433–445. DOI:

639   10.1002/cne.903570308.

640 Henne S., Friedrich F., Hammel JU., Sombke A., Schmidt-Rhaesa A. 2016. Reconstructing the

641   anterior part of the nervous system of Gordius aquaticus (Nematomorpha, cycloneuralia)

642   by a multimethodological approach. *Journal of Morphology* 278:106–118. DOI:

643   10.1002/jmor.20623.

644 Herberholz J., Mims CJ., Zhang X., Hu X., Edwards DH. 2004. Anatomy of a live invertebrate

645   revealed by manganese-enhanced Magnetic Resonance Imaging. *Journal of Experimental*

646   *Biology* 207:4543–4550. DOI: 10.1242/jeb.01328.

647 Holst S., Michalik P., Noske M., Krieger J., Sötje I. 2016. Potential of X-ray micro-computed

648   tomography for soft-bodied and gelatinous cnidarians with special emphasis on

649   scyphozoan and cubozoan statoliths. *Journal of Plankton Research* 38:1225–1242. DOI:

650   10.1093/plankt/fbw054.

651 Kenning M., Harzsch S. 2013. Brain anatomy of the marine isopod *Saduria entomon* Linnaeus,

652   1758 (Valvifera, Isopoda) with special emphasis on the olfactory pathway. *Frontiers in*

653   *Neuroanatomy* 7:1–14. DOI: 10.3389/fnana.2013.00032.

654 Köhnk S., Baudewig J., Brandis D., Boretius S. 2017. What's in this crab? MRI providing high-

655   resolution three-dimensional insights into recent finds and historical collections of

656   Brachyura. *Zoology* 121:1–9. DOI: 10.1016/j.zool.2016.11.004.

657 Krieger J., Braun P., Rivera NT., Schubart CD., Müller CHG., Harzsch S. 2015. Comparative

658   analyses of olfactory systems in terrestrial crabs (Brachyura): evidence for aerial

659   olfaction? *PeerJ* 3:e1433. DOI: 10.7717/peerj.1433.

660 Krieger J., Sombke A., Seefluth F., Kenning M., Hansson BS., Harzsch S. 2012. Comparative

661   brain architecture of the European shore crab *Carcinus maenas* (Brachyura) and the

662   common hermit crab *Pagurus bernhardus* (Anomura) with notes on other marine hermit

663   crabs. *Cell and Tissue Research* 348:47–69. DOI: 10.1007/s00441-012-1353-4.

664   Lang G. 2013. Fixierung. In: *Histotechnik*. Springer Vienna, 47–77. DOI: 10.1007/978-3-7091-

665   1190-1_5.

666   Loesel R., Wolf H., Kenning M., Harzsch S., Sombke A. 2013. Architectural principles and

667   evolution of the arthropod central nervous system. In: Minelli A, Boxshall G, Fusco G

668   eds. *Arthropod Biology and Evolution*. Berlin Heidelberg: Springer, 299–342.

669   Macagno ER., Lopresti V., Levinthal C. 1973. Structure and Development of Neuronal

670   Connections in Isogenic Organisms: Variations and Similarities in the Optic System of

671   Daphnia magna. *Proceedings of the National Academy of Sciences of the United States of*

672   *America* 70:57–61. DOI: 10.1073/pnas.70.1.57.

673   Martin P., Dorn NJ., Kawai T., van der Heiden C., Scholtz G. 2010. The enigmatic Marmorkrebs

674   (marbled crayfish) is the parthenogenetic form of Procambarus fallax (Hagen, 1870).

675   *Contributions to Zoology* 79.

676   Meth R., Wittfoth C., Harzsch S. 2017. Brain architecture of the Pacific White Shrimp Penaeus

677   vannamei Boone, 1931 (Malacostraca, Dendrobranchiata): correspondence of brain

678   structure and sensory input? *Cell and Tissue Research*:1–17. DOI: 10.1007/s00441-017-

679   2607-y.

680   Metscher BD. 2009. MicroCT for comparative morphology: simple staining methods allow high-

681   contrast 3D imaging of diverse non-mineralized animal tissues. *BMC Physiology* 9:11.

682   DOI: 10.1186/1472-6793-9-11.

683   Michalik P., Piacentini L., Lipke E., Ramirez M. 2013. The enigmatic Otway odd-clawed spider

684   (Progradungula otwayensis Milledge, 1997, Gradungulidae, Araneae): Natural history,

685  first description of the female and micro-computed tomography of the male palpal organ.

686  *ZooKeys* 335:101–112. DOI: 10.3897/zookeys.335.6030.

687 Mitchell KJ. 2007. The Genetics of Brain Wiring: From Molecule to Mind. *PLOS Biology*

688  5:e113. DOI: 10.1371/journal.pbio.0050113.

689 Mizutani R., Suzuki Y. 2012. X-ray microtomography in biology. *Micron* 43:104–115. DOI:

690  10.1016/j.micron.2011.10.002.

691 Panel on Animal Health and Welfare. 2005. Opinion of the Scientific Panel on Animal Health

692  and Welfare (AHAW) on a request from the Commission related to the aspects of the

693  biology and welfare of animals used for experimental and other scientific purposes. *EFSA*

694  *Journal* 3:292. DOI: 10.2903/j.efsa.2005.292.

695 O'Sullivan JDB., Behnsen J., Starborg T., MacDonald AS., Phythian-Adams AT., Else KJ.,

696  Cruickshank SM., Withers PJ. 2017. X-ray micro-computed tomography (μCT): an

697  emerging opportunity in parasite imaging. *Parasitology*:1–7. DOI:

698  10.1017/s0031182017002074.

699 Ott SR. 2008. Confocal microscopy in large insect brains: Zinc–formaldehyde fixation improves

700  synapsin immunostaining and preservation of morphology in whole-mounts. *Journal of*

701  *Neuroscience Methods* 172:220–230. DOI: 10.1016/j.jneumeth.2008.04.031.

702 Ott SR., Elphick MR. 2003. New Techniques for Whole-mount NADPH-diaphorase

703  Histochemistry Demonstrated in Insect Ganglia. *Journal of Histochemistry &*

704  *Cytochemistry* 51:523–532. DOI: 10.1177/002215540305100414.

705 Platt KA., Oliver MJ., Thomson WW. 1997. Importance of the Fixative for Reliable

706  Ultrastructural Preservation of Poikilohydric Plant Tissues. Observations on Dry,

707   Partially, and Fully Hydrated Tissues of *Selaginella lepidophylla*. *Annals of Botany*

708   80:599–610. DOI: 10.1006/anbo.1997.0476.

709   Rasmussen KE. 1974. Fixation in aldehydes a study on the influence of the fixative, buffer, and

710   osmolarity upon the fixation of the rat retina. *Journal of Ultrastructure Research* 46:87–

711   102. DOI: 10.1016/S0022-5320(74)80024-9.

712   Richter S., Loesel R., Purschke G., Schmidt-Rhaesa A., Scholtz G., Stach T., Vogt L.,

713   Wanninger A., Brenneis G., Döring C., Faller S., Fritsch M., Grobe P., Heuer CM., Kaul

714   S., Möller OS., Müller CHG., Rieger V., Rothe BH., Stegner MEJ., Harzsch S. 2010.

715   Invertebrate neurophylogeny: suggested terms and definitions for a neuroanatomical

716   glossary. *Frontiers in Zoology* 7:1–49. DOI: 10.1186/1742-9994-7-29.

717   Sandeman DC., Sandeman RE., Derby CD., Schmidt M. 1992. Morphology of the brain of

718   crayfish, crabs, and spiny lobsters: a common nomenclature for homologous structures.

719   *Biological Bulletin* 183:304–326. DOI: 10.2307/1542217.

720   Schmidt M. 2016. Malacostraca. In: Schmidt-Rhaesa A, Harzsch S, Purschke G eds. *Structure &*

721   *Evolution of Invertebrate Nervous Systems*. Oxford: Oxford University Press, 529–582.

722   Snell O. 1891. Die Abhängikeit des Hirngewichtes von dem Körpergewicht und den geistigen

723   Fähigkeiten. *Archiv für Psychiatrie und Nervenkrankheiten* 23:436–446. DOI:

724   10.1007/bf01843462.

725   Sombke A., Lipke E., Michalik P., Uhl G., Harzsch S. 2015. Potential and limitations of X-Ray

726   micro-computed tomography in arthropod neuroanatomy: A methodological and

727   comparative survey. *Journal of Comparative Neurology* 523:1281–1295. DOI:

728   10.1002/cne.23741.

729 Steinhoff POM., Sombke A., Liedtke J., Schneider JM., Harzsch S., Uhl G. 2017. The

730 synganglion of the jumping spider Marpissa muscosa (Arachnida: Salticidae): Insights

731 from histology, immunohistochemistry and microCT analysis. *Arthropod Structure &*

732 *Development* 46:156–170. DOI: 10.1016/j.asd.2016.11.003.

733 Tuchina O., Koczan S., Harzsch S., Rybak J., Wolff G., Strausfeld NJ., Hansson BS. 2015.

734 Central projections of antennular chemosensory and mechanosensory afferents in the

735 brain of the terrestrial hermit crab (*Coenobita clypeatus*; Coenobitidae, Anomura).

736 *Frontiers in Neuroanatomy* 9:1–13. DOI: 10.3389/fnana.2015.00094.

737 Vilpoux K., Sandeman RE., Harzsch S. 2006. Early embryonic development of the central

738 nervous system in the Australian crayfish and the Marbled crayfish (Marmorkrebs).

739 *Development Genes and Evolution* 216:209–223. DOI: 10.1007/s00427-005-0055-2.

740 Vogt G. 2011. Marmorkrebs: Natural crayfish clone as emerging model for various biological

741 disciplines. *Journal of Biosciences* 36:377–382. DOI: 10.1007/s12038-011-9070-9.

742 Ziegler A., Kunth M., Mueller S., Bock C., Pohmann R., Schröder L., Faber C., Giribet G. 2011.

743 Application of magnetic resonance imaging in zoology. *Zoomorphology* 130:227–254.

744 DOI: 10.1007/s00435-011-0138-8.

745

Corrected voxelsizes for cLSM-datasets provided at MorphDBase.

All uploaded datasets lost their original (anisotropic) voxelsize due to conversion of the file format. Note that the voxelsizes given for x/y-axes resulted due to slightly varying optical zooming whereas those for the z-axis were modified by using the correction factor for refractive mismatch in methyl salicylate as immersion medium. Use these voxelsizes to display all cLSM-datasets provided at MorphDBase in the correct spatial scaling.

Method_Fixation	MDB identifier	x/y-voxelsize	z-voxelsize
cLSM_Znfa	M64-001.1	0.702	1.581
cLSM_Znfa	M65-001.1	0.8	1.581
cLSM_Znfa	M67-001.1	0.703	1.581
cLSM_Znfa	M68-001.1	0.84	1.581
cLSM_Znfa	M69-001.1	0.876	1.581
cLSM_Znfa	M70-001.1	0.767	1.581
cLSM_Znfa	M66-001.1	0.881	1.581
cLSM_Glut	M58-001.1	0.722	1.581
cLSM_Glut	M59-001.1	0.868	1.581
cLSM_Glut	M60-001.1	0.868	1.581
cLSM_Glut	M61-001.1	0.737	1.581
cLSM_Glut	M62-001.1	0.682	1.581
cLSM_Glut	M63-001.1	0.755	1.581

Neuronal volumes in *P. fallax* cf. *virginalis* according to the method applied.

Note that corrected volumes use a z-axial correction factor of 1.581 to minimize refractive mismatch due to scanning in methyl salicylate. Abbreviations: DCL, deutocerebral chemosensory lobe; AcN, accessory neuropil (lobe).

Method_Fixation	Stack ID	DCL_R [µm³]	DCL_R corrected [µm³]	DCL_L [µm³]	DCL_L corrected [µm³]	AcN_R [µm³]	AcN_R corrected [µm³]	AcN_L [µm³]	AcN_L corrected [µm³]	Central Brain [µm³]	Central Brain corrected [µm³]	MorphDBase-ID
µCT_Bouin	1	1,486,000		1,576,000		3,646,000		3,667,000		27,713,000		J_Krieger_20170807-M-53-001.1
µCT_Bouin	2	1,699,000		1,600,000		4,129,000		4,649,000		32,730,000		J_Krieger_20170807-M-51-001.1
µCT_Bouin	3	1,555,000		1,388,000		3,789,000		3,417,000		27,083,000		J_Krieger_20170807-M-52-001.1
µCT_Bouin	4	1,274,000		1,274,000		2,942,000		2,896,000		23,533,000		J_Krieger_20170807-M-54-001.1
µCT_Bouin	5	1,515,000		1,389,000		4,809,000		3,955,000		29,820,000		J_Krieger_20170807-M-55-001.1
µCT_Bouin	6	1,585,000		1,554,000		4,292,000		3,990,000		29,373,000		J_Krieger_20170807-M-56-001.1
µCT_Bouin	7	1,171,000		1,171,000		2,646,000		2,696,000		21,071,000		J_Krieger_20170807-M-57-001.1
cLSM_Glut	1	791,003	948,874	883,588	1,059,936	1,907,300	2,287,963	2,010,832	2,412,159	17,744,962	21,286,542	J_Krieger_20170807-M-58-001.1
cLSM_Glut	2	1,041,729	1,249,638	921,645	1,105,587	2,635,866	3,161,934	2,220,232	2,663,347	19,201,752	23,034,055	J_Krieger_20170807-M-59-001.1
cLSM_Glut	3	984,659	1,181,176	1,141,834	1,369,721	2,680,336	3,215,275	2,665,802	3,197,841	19,883,410	23,851,759	J_Krieger_20170807-M-60-001.1
cLSM_Glut	4	1,094,224	1,312,612	1,250,843	1,500,489	3,309,123	3,969,565	3,303,236	3,962,502	27,828,492	33,382,528	J_Krieger_20170807-M-61-001.1
cLSM_Glut	5	1,119,395	1,342,806	1,091,079	1,308,838	2,581,602	3,096,842	2,919,363	3,502,015	21,709,594	26,042,433	J_Krieger_20170807-M-62-001.1
cLSM_Glut	6	1,084,137	1,300,512	1,246,876	1,495,731	2,430,375	2,915,435	2,719,847	3,262,680	20,655,140	24,777,541	J_Krieger_20170807-M-63-001.1
cLSM_ZnFA	1	817,084	980,155	619,376	742,989	2,226,071	2,670,344	1,165,159	1,397,698	18,915,004	22,690,055	J_Krieger_20170807-M-64-001.1
cLSM_ZnFA	2	1,343,450	1,611,573	1,111,938	1,333,857	2,760,117	3,310,976	2,425,304	2,909,342	25,255,030	30,295,377	J_Krieger_20170807-M-65-001.1
cLSM_ZnFA	3	1,419,327	1,070,987	892,802	1,702,596	3,115,787	3,172,392	2,644,587	3,737,634	25,096,024	30,104,705	J_Krieger_20170807-M-66-001.1
cLSM_ZnFA	4	1,198,716	1,437,957	1,161,789	1,393,660	2,756,689	3,306,871	2,440,600	2,927,697	23,043,944	27,643,055	J_Krieger_20170807-M-67-001.1
cLSM_ZnFA	5	1,411,353	1,693,029	1,474,522	1,768,805	3,355,852	4,025,608	3,589,474	4,305,856	27,222,322	32,655,320	J_Krieger_20170807-M-68-001.1
cLSM_ZnFA	7	1,465,908	1,758,472	1,376,278	1,650,954	3,515,581	4,217,219	3,112,145	3,733,264	25,117,220	30,130,071	J_Krieger_20170807-M-69-001.1
cLSM_ZnFA	8	815,546	1,086,852	906,027	978,312	2,123,881	2,651,125	2,210,045	2,547,765	15,918,198	19,095,127	J_Krieger_20170807-M-70-001.1

Brain volumes of six adult specimens of *P. fallax* cf. *virginalis* during three stages of sample preparation for µCT-scanning.

Stage 1) freshly dissected brain scanned moistly in water; stage 2) after fixation in Bouin's solution but without dehydration or contrast enhancement; stage 3) after fixation, dehydration in ethanol and contrast enhancement in 2 % iodine.

Method_ Fixation	Specimen ID	Central Brain [µm³]	MorphDBase-ID
µCT_stage_1	1	3,390,200,000	J_Krieger_20180329-M-71-001.1
µCT_stage_2	1	3,044,452,000	J_Krieger_20180329-M-77-001.1
µCT_stage_3	1	3,224,483,000	J_Krieger_20180329-M-83-001.1
µCT_stage_1	2	6,524,711,000	J_Krieger_20180329-M-72-001.1
µCT_stage_2	2	6,010,940,000	J_Krieger_20180329-M-78-001.1
µCT_stage_3	2	6,409,148,000	J_Krieger_20180329-M-84-001.1
µCT_stage_1	3	6,548,093,000	J_Krieger_20180329-M-73-001.1
µCT_stage_2	3	5,544,624,000	J_Krieger_20180329-M-79-001.1
µCT_stage_3	3	5,022,508,000	J_Krieger_20180329-M-85-001.1
µCT_stage_1	4	7,620,066,000	J_Krieger_20180329-M-74-001.1
µCT_stage_2	4	4,925,074,000	J_Krieger_20180329-M-80-001.1
µCT_stage_3	4	5,451,010,000	J_Krieger_20180329-M-86-001.1
µCT_stage_1	5	6,041,379,000	J_Krieger_20180329-M-75-001.1
µCT_stage_2	5	3,333,409,000	J_Krieger_20180329-M-81-001.1
µCT_stage_3	5	3,098,399,000	J_Krieger_20180329-M-87-001.1
µCT_stage_1	6	7,333,405,000	J_Krieger_20180329-M-76-001.1
µCT_stage_2	6	4,984,792,000	J_Krieger_20180329-M-82-001.1
µCT_stage_3	6	5,115,247,000	J_Krieger_20180329-M-88-001.1

Average volume of deutocerebral chemosensory lobe (single lobe) of various decapod species.

Asterisks indicate resulting volumes using the correction factor for methyl salicylate provided as immersion medium by Bucher et al. (2000).

Taxon	Species	n	DCL volume [mm³] *with optical correction	Reference
Astacida	*Procambarus fallax* cf. *virginalis* (juv.)	7	0.0015	this study (µCT)
Astacida	*Procambarus fallax* cf. *virginalis* (juv.)	7	0.0011/*0.0014	this study (ZnFA)
Astacida	*Procambarus fallax* cf. *virginalis* (juv.)	6	0.0011/*0.0013	this study (Karnofsky)
Astacida	*Procambarus clarkii* (adult)	3	0.0097	Beltz et al. 2003
Homarida	*Homarus americanus* (adult)	2	0.1412	Beltz et al. 2003
Anomala	*Birgus latro* (adult)	1	0.3747	Krieger et al. 2012
Brachyura	*Sesarma* sp. (adult)	3	0.0061	Beltz et al. 2003

Figure 1

Volumes of brain compartiments according to the methods applied.

Boxplots with median, upper and lower quartiles, minima and maxima, and outliers of volumes of the deutocerebral chemosensory lobes (DCLs) in A, the accessory lobe (AcNs) in B, and the central brain in C. Note that the displayed volumes for DCLs and AcNs refer to the total volumes of both brain hemispheres. All volumetric data of cLSM-scanning resulted from z-corrected datasets using the correction factor for refractive mismatch with methyl salicylate provided by Bucher et al. (2000).
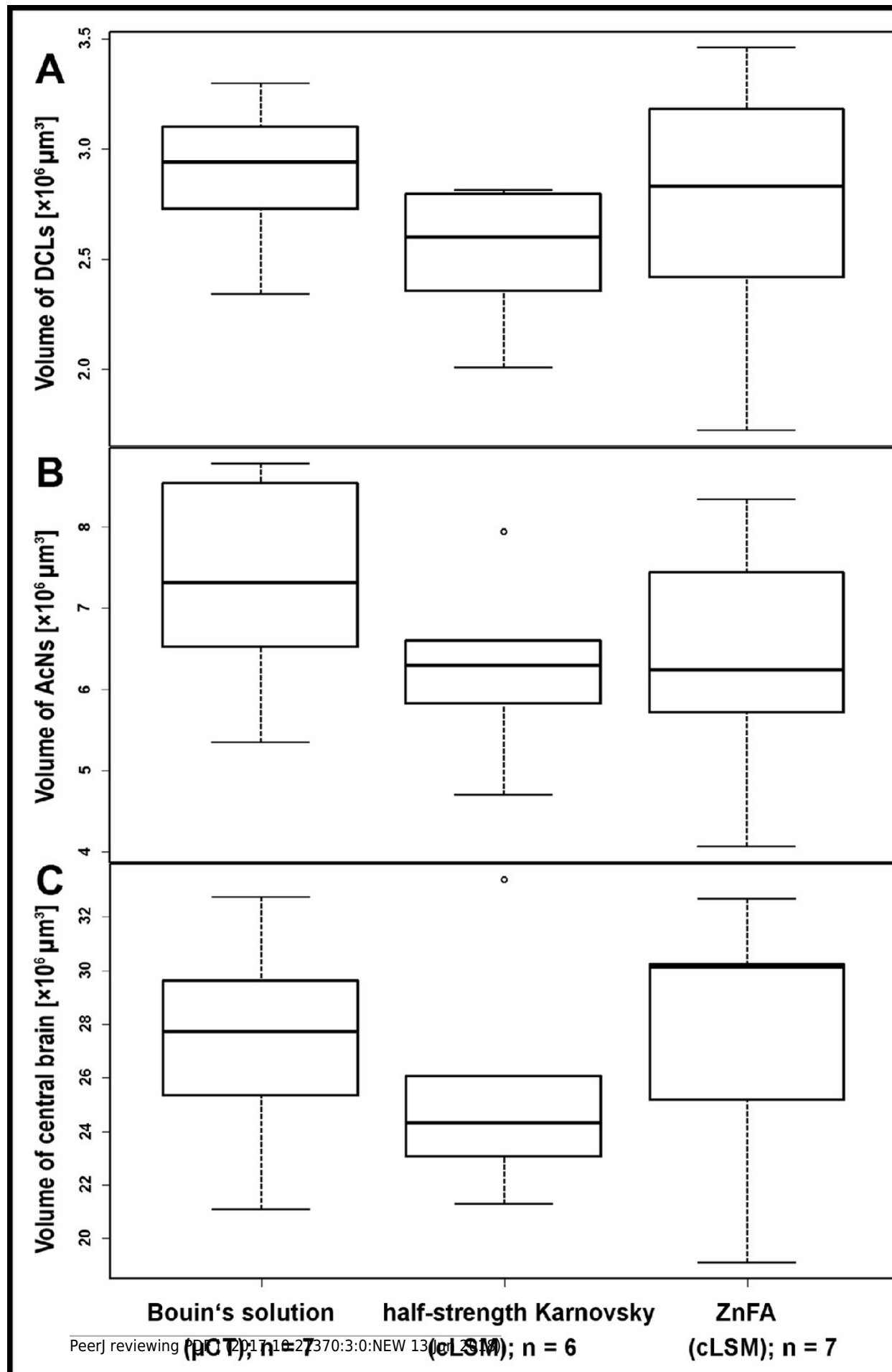
Figure 2

Comparison of volumetric data based on the methodologic approach of *P. fallax* cf. *virginalis.*

Each bar represents the average of reconstructed volumes of deutocerebral chemosensory lobes (DCLs), accessory lobes (ACNs), as well as of the central brain of all specimens analyzed. Note that volumes of the DCLs as well as of the AcNs are plotted pairwise (both brain hemispheres per specimen). Applied methods: μCT (Bouin-fixation), cLSM (half-strength Karnovsky's solution), and cLSM (ZnFA-fixation). The levels of significance between pairs of volumes of brain substructures according to the methods applied are based on Tukey's post-hoc test from a one-way analysis of variance (ANOVA). Note that all cLSM volumes include the correction factor for refractive mismatch for methyl salicylate from Bucher et al. (2000).

Volumetric comparison of brain substructures according to the method applied

☐ Bouin (µCT); n = 7
▨ half-strength Karnovsky's solution (cLSM); n = 6
■ ZnFA (cLSM); n = 7

Y-axis: Volume of DCLs [×10^6 µm³] — 0, 10, 20, 30, 40

X-axis categories: DCLs, AcNs, central brain
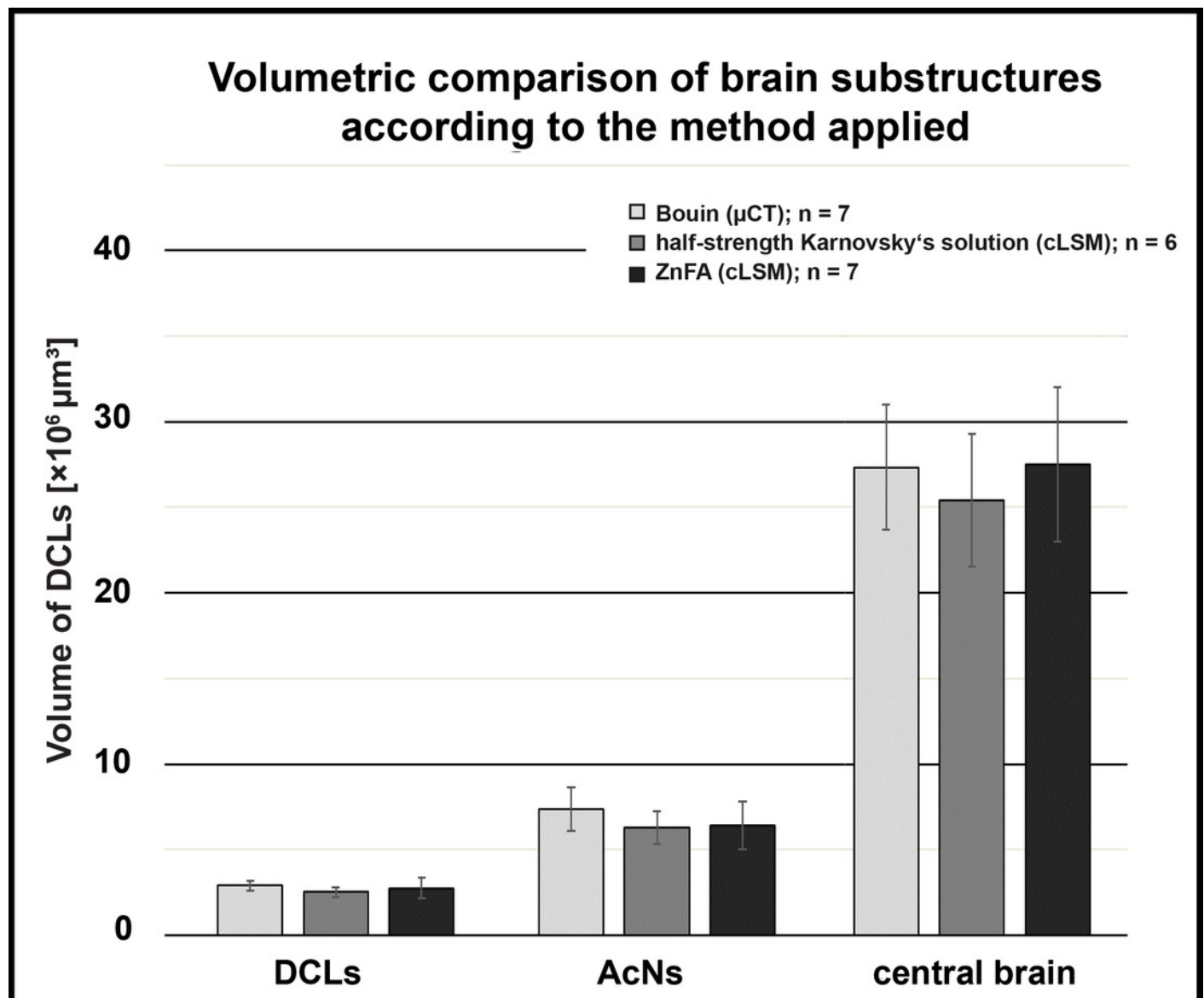
u# Figure 3

Volume renderings of the brain in *P. fallax* cf. *virginalis* from a μCT-scan.

The outline of the whole animal body is visualized in A, while in B, a virtual cutaway reveals the position of the brain (white area indicated by a black arrow) from the same perspective. The color-labeled areas in C and D are based on surface reconstruction and show the central brain (orange), the deutocerebral chemosensory lobes (DCLs: green), and the accessory lobes (AcNs: purple). Note that the lateral protocerebrum (latPC) is not reconstructed but visible in dark gray in C and D beneath the ommatidia of the complex-eyes (ce). Other abbreviations: AI, antenna 1 (antennule); AII, antenna 2 (antenna); OC, oesophageal connective.

vvvvvrts
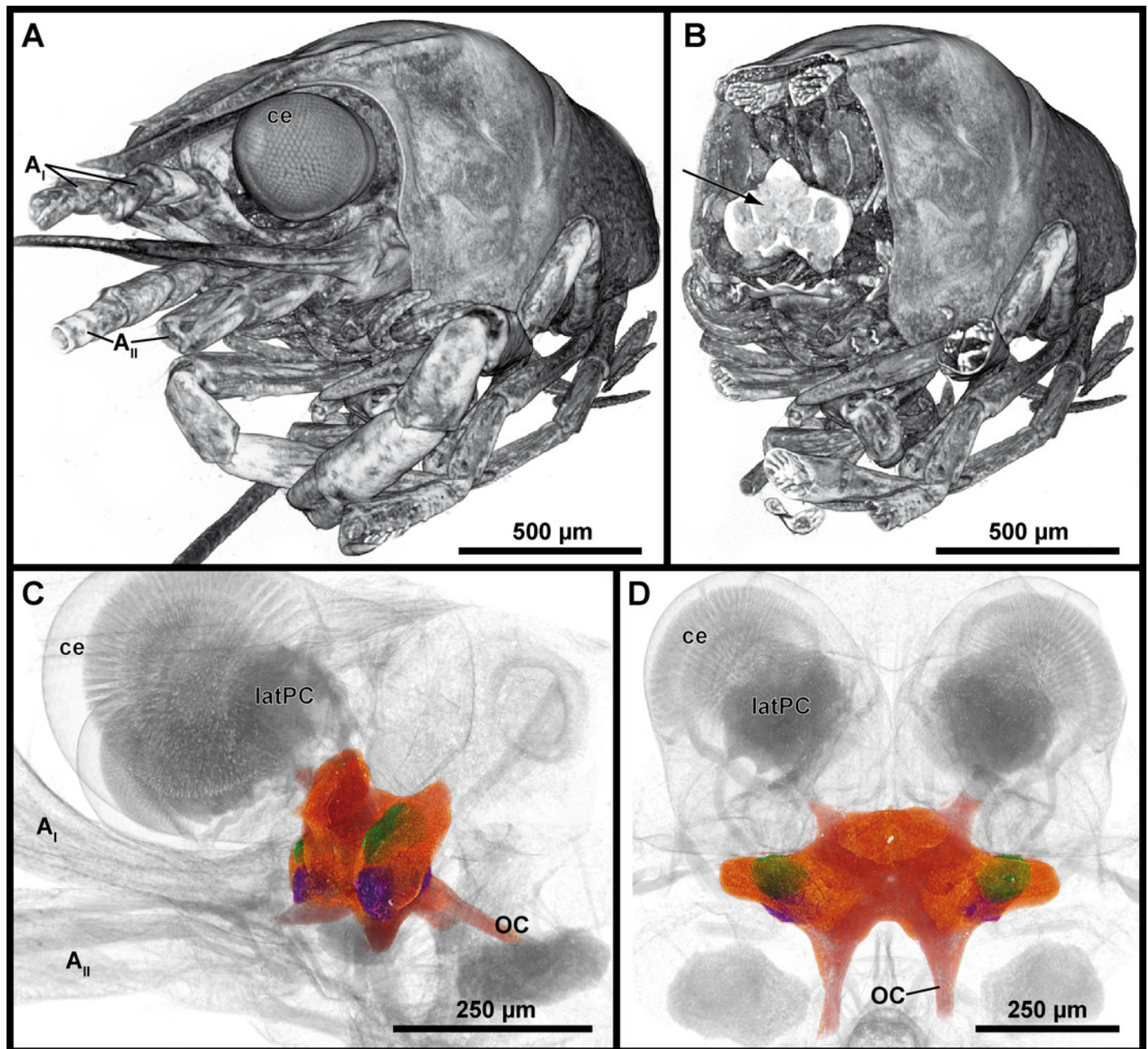
Figure 4

Comparison of virtual brain sections of *P. fallax* cf. *virginalis* based on all three methods applied.

The scheme in A illustrates the general organization of the central brain (omitting the lateral protocerebrum, nerves, and the oesophageal connectives). Frontal virtual sections of the central brain, according to the tomographic and corresponding fixing method applied, are shown equally scaled in B (µCT using Bouin's solution); in C (cLSM using autofluorescence of half-strength Karnovsky's solution); and in D (cLSM using ZnFA and immunohistochemical labeling against synapsin). Abbreviations: AcN, accessory neuropil; AMPN, anterior medial protocerebral neuropil; AnN, Antenna-II-neuropil; CA, cerebral artery; CB, central body, DCL, deutocerebral chemosensory lobe (olfactory lobe); LAN, lateral antenna-I-neuropil; MAN, median antenna-I-neuropil; PB, protocerebral bridge; PMPN, posterior medial protocerebral neuropil; PNT, projection neuron tract; TN, tegumentary neuropil; 6, 9/11, and 10 indicate somata clusters (6), (9/11), and (10); asterisk indicates olfactory glomeruli in A, C, and D.
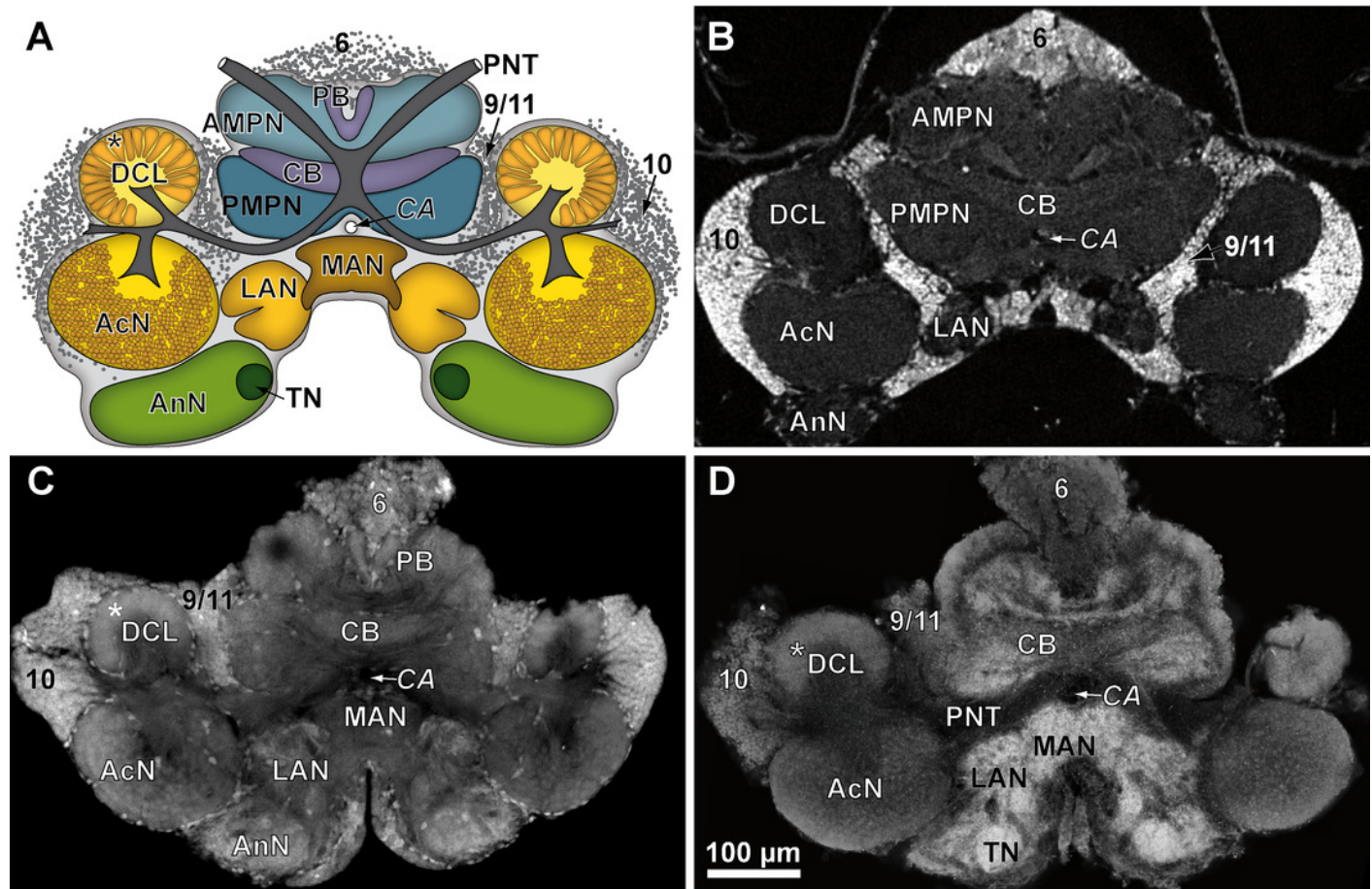
Figure 5

Virtual sections of adult individual of *P. fallax* cf. *virginalis* and volumes of central brains after different preparation stages.

(A) Boxplots with median, upper, and lower quartiles, minima and maxima, and outliers of volumes of the central brain after different stages of preparation for µCT wet-scanning. (B) Frontal virtual slices of the central brain of an adult individual of *P. fallax* cf. *virginalis*. Stage 1) The brains are just dissected and immediately scanned in tap water. Stage 2) Brains are fixed in Bouin's solution. Stage 3) Gradual dehydration and contrast enhancement with iodine (2%) *: Significant difference between stage 1 and 2,3 (Wilcoxon signed rank test: p = 0.0313; n = 6) ns: No significant difference between stage 2 and 3 (Wilcoxon signed rank test: p = 0.6875; n = 6).
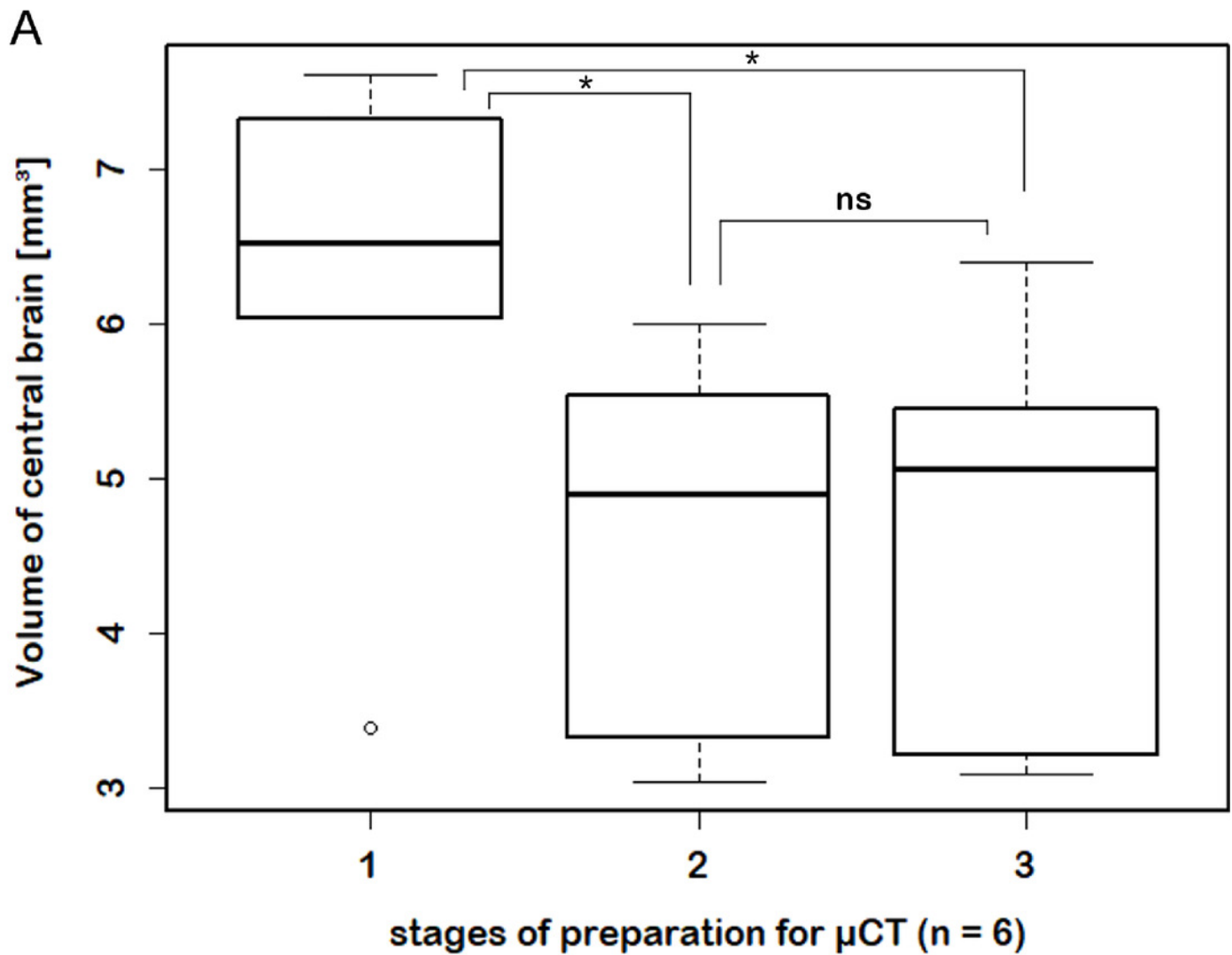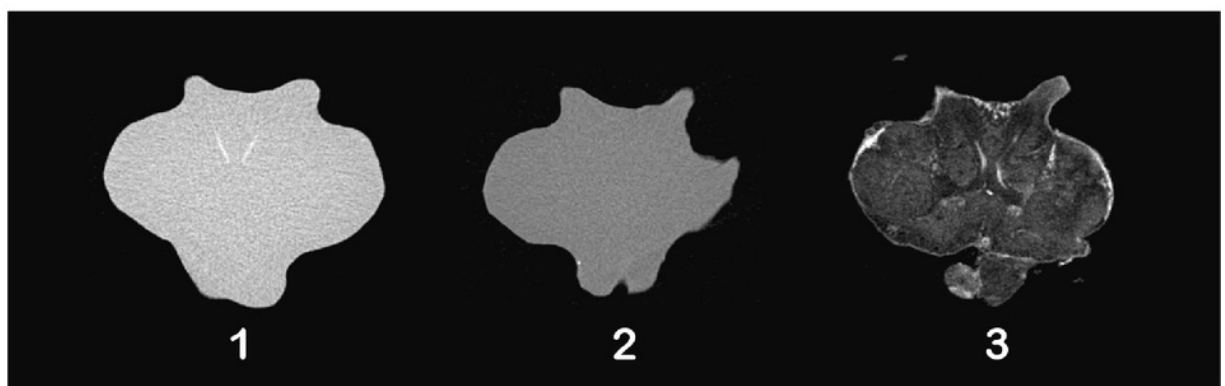
Figure 6

Comparison of grayscale-based surface reconstructions of the central brain of two individuals of *P. fallax* cf. *virginalis.*

The isosurfaces are based on confocal laser-scanning microscopy of dissected brains fixed in half-strength Karnovsky's solution (A-C) and in ZnFA (D-F), and are shown from different perspectives (A and D: from anterioventral; B and E: from posteriodorsal; C and F: from ventrolateral). Abbreviations: AIINv, antenna 2-nerve; AcN, accessory neuropil; AnN, antenna 2-neuropil; DCL, deutocerebral chemosensory lobe (olfactory lobe); LAN, lateral antenna 1-neuropil; mPC, median protocerebrum; OC, oesophageal connective.

A

mPC

A$_{II}$Nv

LAN

AnN

B

DCL

AcN

C

DCL

A$_{II}$Nv

AcN

D

A$_{II}$Nv

mPC

AnN

OC

E

DCL

OC

F

A$_{II}$Nv

DCL

AcN

OC